



Highly-efficient laser operation of a novel trigonal silicate crystal $\text{Yb}^{3+}:\text{Ca}_3\text{NbGa}_3\text{Si}_2\text{O}_{14}$

XUZHAO ZHANG,^{1,2} PAVEL LOIKO,³ JOSEP MARIA SERRES,¹ XAVIER MATEOS,^{1,4,*} JUNYU REN,² ZHENGPING WANG,² SHIYI GUO,² XINGUANG XU,^{2,6} ELENA VILEJSHIKOVA,⁵ UWE GRIEBNER,⁴ VALENTIN PETROV,⁴ MAGDALENA AGUILÓ,¹ AND FRANCESC DÍAZ¹

¹*Física i Cristal·lografia de Materials i Nanomaterials (FiCMA-FiCNA)-EMaS, Dept. Química Física i Inòrganica, Universitat Rovira i Virgili (URV), Campus Sescelades, E-43007 Tarragona, Spain*

²*State Key Laboratory of Crystal Materials and Institute of Crystal Materials, Shandong University, 250100 Jinan, China*

³*ITMO University, 49 Kronverkskiy pr., 197101 St. Petersburg, Russia*

⁴*Max Born Institute for Nonlinear Optics and Short Pulse Spectroscopy, Max-Born-Str. 2a, D-12489 Berlin, Germany*

⁵*Center for Optical Materials and Technologies, Belarusian National Technical University, 65/17 Nezavisimosti Ave., 220013 Minsk, Belarus*

⁶*xgxu@sdu.edu.cn*

**xavier.mateos@urv.cat*

Abstract: A novel trigonal ordered langasite-type silicate crystal, $\text{Yb}^{3+}:\text{Ca}_3\text{NbGa}_3\text{Si}_2\text{O}_{14}$ (Yb:CNGS), is characterized with respect to absorption and stimulated-emission cross-sections as well as Raman spectra using polarized light. Thanks to its excellent thermo-mechanical properties, highly-efficient multi-watt lasing is demonstrated. A compact *a*-cut 5 at .% Yb:CNGS crystal diode-pumped at 978 nm generated a maximum output power of 7.27 W at 1062–1068 nm with a slope efficiency of 78%. These values represent record parameters for ~ 1 μm lasers based on langasite-type crystals. The very broad and smooth gain cross sections of Yb:CNGS are attractive for ultrashort pulse and broadly tunable lasers at ~ 1 μm .

© 2017 Optical Society of America

OCIS codes: (140.3380) Laser materials; (300.0300) Spectroscopy; (140.3480) Lasers, diode-pumped.

References and links

1. M. Jacquemet, C. Jacquemet, N. Janel, F. Druon, F. Balembis, P. Georges, J. Petit, B. Viana, D. Vivien, and B. Ferrand, "Efficient laser action of Yb:LSO and Yb:YSO oxyorthosilicates crystals under high-power diode-pumping," *Appl. Phys. B* **80**(2), 171–176 (2005).
2. T. L. Feng, S. Z. Zhao, K. J. Yang, G. Q. Li, D. C. Li, J. Zhao, W. C. Qiao, J. Hou, Y. Yang, J. L. He, L. H. Zheng, Q. G. Wang, X. D. Xu, L. B. Su, and J. Xu, "Diode-pumped continuous wave tunable and graphene Q-switched Tm:LSO lasers," *Opt. Express* **21**(21), 24665–24673 (2013).
3. K. Shimamura, H. Takeda, T. Kohno, and T. Fukuda, "Growth and characterization of lanthanum gallium silicate $\text{La}_3\text{Ga}_5\text{SiO}_{14}$ single crystals for piezoelectric applications," *J. Cryst. Growth* **163**(4), 388–392 (1996).
4. Z. M. Wang, X. F. Cheng, D. R. Yuan, L. H. Pan, S. Y. Guo, D. Xu, and M. K. Lv, "Crystal growth and properties of $\text{Ca}_3\text{NbGa}_3\text{Si}_2\text{O}_{14}$ single crystals," *J. Cryst. Growth* **249**(1–2), 240–244 (2003).
5. I. H. Jung, A. Yoshikawa, T. Fukuda, and K. H. Auh, "Growth and structure of $\text{A}_3\text{NbGa}_3\text{Si}_2\text{O}_{14}$ (A = Sr, Ca) compounds," *J. Alloys Compd.* **339**(1–2), 149–155 (2002).
6. X. Zhang, Y. Zhou, J. Ren, D. Lu, H. Yu, Z. Wang, S. Guo, and X. Xu, "Growth, thermal and laser properties of a new self-frequency doubling Yb:CNGS crystal," *CrystEngComm* **18**(28), 5338–5343 (2016).
7. Y. Yu, J. Wang, H. Zhang, Z. Wang, H. Yu, and M. Jiang, "Continuous wave and Q-switched laser output of laser-diode-end-pumped disordered Nd:LGS laser," *Opt. Lett.* **34**(4), 467–469 (2009).
8. Q. Wang, Z. Wei, Y. Zhang, Z. Zhang, H. Yu, H. Zhang, J. Wang, M. Gao, C. Gao, and Z. Wang, "Tunable continuous-wave laser at quasi-three-level with a disordered Nd:LGS crystal," *Opt. Lett.* **36**(10), 1770–1772 (2011).
9. X. Zhang, X. Zhang, S. Guo, J. He, K. Han, F. Lou, B. Zhang, R. Wang, and X. Liu, "Growth and optical properties of a new CGG-type laser crystal $\text{Nd}^{3+}:\text{CNGS}$," *Opt. Mater. Express* **5**(5), 977–985 (2015).
10. J. Ren, X. Zhang, X. Zhang, J. Guo, R. Cheng, and S. Guo, "Growth and enhanced electro-elastic properties of $\text{Nd}^{3+}:\text{CNGS}$ crystals with ordered langasite structure," *Mater. Lett.* **167**, 122–124 (2016).

11. J. Li, X.-T. Zhang, J.-L. He, S. Guo, J. Ning, F. Lou, R. Zhao, X.-C. Su, J. Hou, and B.-T. Zhang, "759 fs pulse generation with Nd³⁺-doped CNGS ordered crystal based on a semiconductor saturable absorber mirror," *Appl. Opt.* **55**(20), 5444–5448 (2016).
12. B. V. Mill, E. L. Belokoneva, and T. Fukuda, "New compounds with Ca₃Ga₂Ge₄O₁₄-type structure: A₃XY₃Z₂O₁₄ (A=Ca, Sr, Ba, Pb; X=Sb, Nb, Ta; Y=Ga, Al, Fe, In; Z=Si, Ge)," *Russ. J. Inorg. Chem.* **43**(8), 1168–1175 (1998).
13. J. Ren, X. Zhang, X. Zhang, R. Cheng, J. Guo, X. Zhang, F. Yu, B. Huang, and S. Guo, "Crystal growth, experimental and theoretical studies on the electronic structure of CNGS and Nd:CNGS," *CrystEngComm* **18**(19), 3481–3487 (2016).
14. J. Lan, G. Lu, Z. Wang, G. Zhu, D. Yuan, and H. Xia, "Raman scattering spectra of Ca₃NbGa₃Si₂O₁₄ (CNGS) crystals," *Phys. Status Solidi* **242**(10), 1996–2004 (2005).
15. A. S. Yasyukevich, V. G. Shcherbitskii, V. E. Kisel, A. V. Mandrik, and N. V. Kuleshov, "Integral method of reciprocity in the spectroscopy of laser crystals with impurity centers," *J. Appl. Spectrosc.* **71**(2), 202–208 (2004).
16. J. M. Serres, P. Loiko, X. Mateos, K. Yumashev, N. Kuleshov, V. Petrov, U. Griebner, M. Aguiló, and F. Díaz, "Prospects of monoclinic Yb:KLu(WO₄)₂ crystal for multi-watt microchip lasers," *Opt. Mater. Express* **5**(3), 661–667 (2015).
17. R. Lan, P. Loiko, X. Mateos, Y. Wang, J. Li, Y. Pan, S. Y. Choi, M. H. Kim, F. Rotermund, A. Yasyukevich, K. Yumashev, U. Griebner, and V. Petrov, "Passive Q-switching of microchip lasers based on Ho:YAG ceramics," *Appl. Opt.* **55**(18), 4877–4887 (2016).
18. P. Loiko, J. M. Serres, X. Mateos, H. Yu, H. Zhang, J. Liu, K. Yumashev, U. Griebner, V. Petrov, M. Aguiló, and F. Díaz, "Thermal lensing and multi-watt microchip laser operation of Yb:YCOB crystals," *IEEE Photonics J.* **8**(3), 1501312 (2016).

1. Introduction

Silicates are known as very suitable laser host crystals for doping with trivalent rare-earth ions (RE³⁺). A well-known example is the family of monoclinic RE₂SiO₅ silicates that allows for the incorporation of Nd³⁺, Yb³⁺, Er³⁺ or Tm³⁺ leading to efficient laser operation in the near-IR [1,2]. There exists a different class of langasite-type trigonal silicate crystals. Lanthanum gallium silicate (langasite) La₃Ga₅SiO₁₄ (LGS) [3], and calcium niobium gallium silicate, Ca₃NbGa₃Si₂O₁₄ (CNGS) [4] belong to this class. These crystals are known for their good elastic and thermal properties and they were studied as piezoelectric materials [3]. LGS has a disordered structure while CNGS is an ordered crystal that is mechanically stronger and possesses better elastic properties than LGS [5]. CNGS exhibits weak thermal expansion ($\alpha_a = 5.7$ and $\alpha_c = 5.5 \times 10^{-6} \text{ K}^{-1}$), high specific heat ($C_p = 0.83 \text{ J/gK}$) and moderate thermal conductivity ($\kappa = 1.82 \text{ W/mK}$) [6]. Therefore, it is very interesting for RE³⁺ doping concerning power-scaling. The acentric (point group 32) CNGS crystals are suitable for self-frequency-doubling (SFD) [6].

To date, only few studies were devoted to RE³⁺-doped LGS and CNGS crystal lasers focusing mostly on Nd³⁺ ions and reporting modest output characteristics. Continuous-wave (CW) and passively Q-switched (PQS) Nd:LGS lasers were demonstrated [7,8]. Later on, the spectroscopic, elastic and laser properties of Nd:CNGS crystal were described [9,10]. The Nd:CNGS laser generated 1.63 W at 1065 nm with a slope efficiency η of 31%. Mode-locking of a Nd:CNGS laser was also demonstrated very recently [11].

Ytterbium (Yb³⁺) doping is very suitable for highly-efficient and power-scalable lasers at $\sim 1 \mu\text{m}$. This is due to the simple energy-level scheme of the Yb³⁺ ion eliminating parasitic mechanisms such as excited-state absorption and upconversion. Yb³⁺ ions are typically excited at the ${}^2F_{7/2} \rightarrow {}^2F_{5/2}$ transition by commercial InGaAs laser diodes emitting at ~ 960 – 980 nm leading to a low quantum defect. When embedded in anisotropic matrices, the Yb³⁺ ions offer broad spectral bands leading to wavelength-tunable laser emission [1]. Yb³⁺-doped CNGS crystals have been grown only very recently [6]. Besides the crystal growth, this first work reported on the thermal properties, preliminary laser operation and SFD characterization.

In the present paper, we demonstrate the potential of Yb:CNGS for highly-efficient multi-watt CW laser operation based on a polarization-resolved study of the spectroscopic properties.

2. Crystal growth and spectroscopy

CNGS melts congruently at ~ 1350 °C [4]. High optical quality 1 at.%, 3 at.% and 5 at.% Yb:CNGS crystals were grown by the Czochralski pulling method in a $N_2 + 1$ vol% O_2 atmosphere (in order to avoid formation of color centers related to the oxygen defects) using [100]-oriented CNGS seeds. The as-grown and polished 5 at.% Yb:CNGS crystal is shown in Fig. 1(a). It had a slight yellow coloration due to the weak absorption band at ~ 460 nm related to the residual O defects, Fig. 1(b), which can be partially removed by a proper annealing in air, see inset in Fig. 1(b).

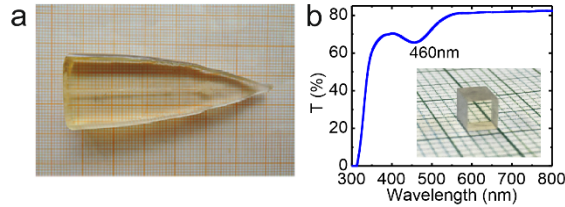


Fig. 1. 5 at.% Yb:CNGS crystal: (a) Photograph of the as-grown bulk; (b) transmission spectrum (T) of an a -cut 4-mm thick sample in the visible, *inset*: image of this sample.

The structure and phase purity of the crystals were confirmed by X-ray powder diffraction (XRD). Yb:CNGS is trigonal (sp. gr. $P321$, lattice constants $a = b = 8.0779$ Å, $c = 4.9750$ Å) and belongs to the family of $A_3BGa_3Si_2O_{14}$ crystals where $A = Ca$ or Sr and $B = Ta$ or Nb with a langasite-type but ordered structure [12]. In the CNGS lattice, Fig. 2(a), the Ca^{2+} ions are located in a twisted Thomson cube ($3e$ Wyckoff position, VIII-fold O^{2-} -coordination, ionic radius $R_{Ca} = 1.12$ Å) with relatively large $Ca^{2+} - O^{2-}$ distances, $2.22 - 2.83$ Å [5]. The edge-sharing $[CaO_8]$ polyhedra form isolated planes parallel to the a - b plane linked by $[GaO_4]$ and $[SiO_4]$ tetrahedra. The Yb^{3+} ions ($R_{Yb} = 0.985$ Å) in CNGS will replace the Ca^{2+} ones providing a certain number of A vacancies to maintain the charge compensation [6,13]. Small Yb^{3+} ions in the A sites will further stabilize the CNGS structure [5].

CNGS is an optically uniaxial crystal. Its optical axis is parallel to the c -axis. The principal refractive indices, $n_o = 1.772$ and $n_e = 1.855$ at 1.02 μm [9] (positive uniaxial crystal). The two principal light polarizations for Yb:CNGS are $E \parallel c$ (π) and $E \perp c$ (σ).

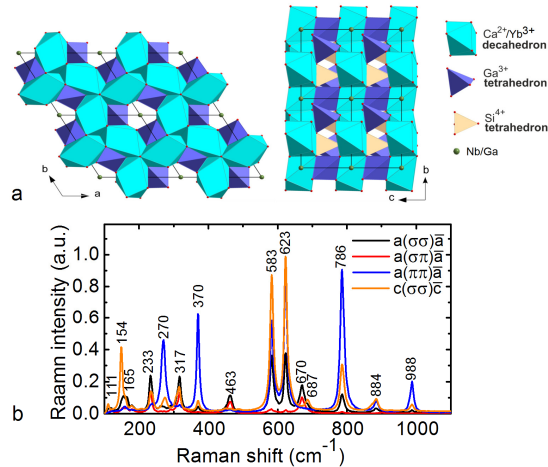


Fig. 2. Structural study of a 5 at.% Yb:CNGS crystal: (a) fragment of the CNGS structure in projection to the a - b and b - c planes; (b) polarized Raman spectra, $\lambda_{exc} = 514$ nm.

The structure of Yb:CNGS was further studied by Raman spectroscopy. The polarized Raman spectra of a 5 at.% Yb:CNGS crystal for the $a(\sigma\sigma)\bar{a}$, $a(\sigma\pi)\bar{a}$, $a(\pi\pi)\bar{a}$ and $c(\sigma\sigma)\bar{c}$

geometries are shown in Fig. 2(b). They were measured with a Renishaw inVia confocal Raman microscope, the excitation wavelength $\lambda_{\text{exc}} = 514$ nm. The standard $m(nk)\bar{l}$ notations are used (m and l are the propagation directions of the excitation and scattered light, and $m \equiv l$ for the confocal geometry used, n and k are the polarizations of the excitation and scattered light, respectively). The spectra agree well with those for the undoped CNGS [14]. At the center point (Γ) of the first Brillouin zone, the irreducible representations can be written as $\Gamma = 10A_1 + 13A_2 + 23E$, of which $1A_2 + 1E$ modes are acoustic, $10A_1$ modes are Raman-active, $12A_2$ ones are IR-active and the rest of $22E$ ones are either Raman or IR-active. A total of 15 modes are clearly resolved in Fig. 2(b). The maximum phonon frequency of Yb:CNGS is 988 cm^{-1} (A_1) and it is assigned to the Si-O stretching vibrations. The most intense bands in the Raman spectra are located at 583 (A_1), 623 (A_1) and 786 (A_1) cm^{-1} and are related to the O-Si-O bending, O-Ga-O stretching and Si-O stretching vibrations, respectively.

At first, we studied the spectroscopic properties of a 5 at.% Yb:CNGS crystal. The Yb³⁺ doping concentration N_{Yb} was calculated as 5.3×10^{20} at/cm^3 assuming a segregation coefficient $K_{\text{Yb}} \approx 1$ and a density $\rho = 4.17$ g/cm^3 (measured with a hydrostatic method). The absorption spectra were measured using a Varian CARY-5000 spectrophotometer; the spectral bandwidth (SBW) was 0.3 nm. The absorption cross-sections, σ_{abs} , for π and σ -polarizations are shown in Fig. 3(a). A specific feature of the absorption spectrum is the presence of two closely located peaks centered at 977.2 and 979.1 nm and clearly resolved even at RT. It was not reported in [6] due to the low resolution spectral measurements. According to the low-temperature (6 K) spectroscopy (unpublished), they are related to the transitions from two closely located Stark sub-levels of the $^2F_{7/2}$ ground-state (transitions $0 \rightarrow 0'$ (zero-phonon line, ZPL), and $1 \rightarrow 0'$, respectively). The maximum σ_{abs} is 1.3×10^{-20} cm^{-2} at 979.1 nm and the total full width at half maximum (FWHM) of the absorption peak around the ZPL is 4.2 nm (for σ -polarization).

The stimulated-emission cross-sections, σ_{SE} , were calculated with the modified reciprocity method [15]:

$$\sigma_{\text{SE}}^i(\lambda) = \frac{1}{8\pi n_i^2 \tau_{\text{Yb}} c} \frac{3\sigma_{\text{abs}}^i(\lambda)e^{-hc/(kT\lambda)}}{\sum_{i=\pi,\sigma} \int \lambda^{-4} \sigma_{\text{abs}}^i(\lambda)e^{-hc/(kT\lambda)} d\lambda}, \quad (1)$$

where $i = \pi$ or σ denotes the polarization, c is the speed of light, τ_{Yb} is the $^2F_{5/2}$ lifetime of the Yb³⁺ ions. The results are presented in Fig. 3(a).

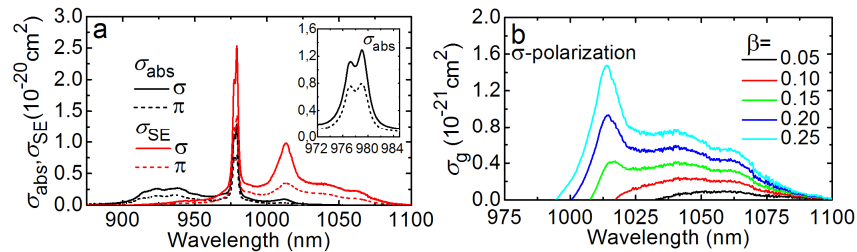


Fig. 3. Spectroscopy of the trigonal Yb:CNGS crystal: (a) absorption, σ_{abs} , and stimulated-emission, σ_{SE} , cross-sections for π and σ -polarizations, *inset* – the spectrum around the ZPL; (b) gain cross-sections, $\sigma_g = \beta\sigma_{\text{SE}} - (1 - \beta)\sigma_{\text{abs}}$, for σ -polarization, β is the inversion ratio, $\beta = N_2/N_{\text{Yb}}$.

The Yb:CNGS crystal exhibits a strong polarization-anisotropy of the σ_{SE} spectra which is a prerequisite for the linearly polarized laser output. The larger σ_{SE} is observed for σ -polarization: the maximum is $\sigma_{\text{SE}} = 2.5 \times 10^{-20}$ cm^{-2} at 979.1 nm and in the spectral range of highest gain cross section at ~ 1018 nm, it is 0.97×10^{-20} cm^{-2} . This is lower than the

estimation from [6] due to the low resolution spectral measurements not accounting for the reabsorption effect on the emission spectra [6].

The Yb^{3+} ion represents a quasi-three-level laser scheme and the emission wavelength is determined by the level of inversion, $\beta = N_2(^2F_{5/2})/N_{\text{Yb}}$, in accordance with the gain cross-section, $\sigma_g = \beta\sigma_{\text{SE}} - (1 - \beta)\sigma_{\text{abs}}$, spectra, as shown in Fig. 3(b) for σ -polarization. For small $\beta < 0.15$, the gain spectrum is smooth and broad with a potential bandwidth of >80 nm. Increasing β , a local peak is formed in the spectrum centered at ~ 1018 nm ($\beta > 0.15$). Thus, this material may be of interest for broadband tunable and ultrashort pulse lasers. The luminescence decay curve was measured from an edge of a 1 at.% Yb:CNGS crystal (thickness: 3 mm) to avoid reabsorption effect and it is shown in Fig. 4. It is clearly single-exponential; the decay time τ_{lum} is 0.71 ms.

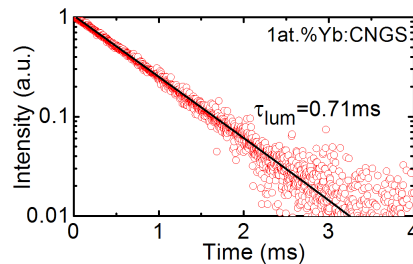


Fig. 4. Luminescence decay curve for a 1 at.% Yb:CNGS crystal: circles – experimental data, black curve – single-exponential fit. Duration of the excitation pulse – 5 ns.

3. Microchip laser operation

The laser experiments were performed in a compact (microchip type) set-up [16]. The uncoated crystal was mounted in a Cu-holder providing cooling from all four lateral sides and Indium foil ensured good thermal contact. The holder was water-cooled down to 14 °C. The plano-plano cavity consisted of a pump mirror (PM) antireflection (AR)-coated for 0.88–0.99 μm and high-reflection (HR)-coated for 1.01–1.23 μm , and an output coupler (OC) providing transmittance $T_{\text{OC}} = 0.5\%$, 1%, 5% or 10% for 1.02–1.1 μm . Both PM and OC were located as close as possible to the polished crystal faces, i.e. with minimum air gaps. Hence the geometrical cavity length was almost equal to the thickness of the Yb:CNGS sample.

As pump source, we used an InGaAs fiber coupled laser diode (fiber core diameter: 200 μm ; numerical aperture N.A.: 0.22) emitting up to ~ 20 W at ~ 978 nm. The unpolarized pump radiation ($M^2 \sim 71$) was collimated and focused into the crystal using a lens assembly (1:1 imaging ratio, focal length: 30 mm) resulting in a pump spot radius w_p of ~ 100 μm and a Rayleigh length of $2z_R = 1.65$ mm (in the crystal). All four OCs provided partial reflection at the pump wavelength ($\sim 90\%$), so the crystal was pumped in a double-pass. The total pump absorption under lasing conditions ($Abs = P_{\text{abs}}/P_{\text{inc}}$, where P_{abs} and P_{inc} are the absorbed and incident pump power, respectively) was determined from the small-signal pump-transmission measurements and rate-equation modelling [17].

In all laser experiments, we studied a -cut samples in order to maintain linearly polarized laser output. At first, we studied the effect of the output coupling on the laser performance, using a 3 mm-thick 3 at.% Yb:CNGS crystal that provided an Abs of $\sim 41\%$, see Fig. 5(a). The best performance was observed for $T_{\text{OC}} = 1\%$, namely 3.16 W at 1054–1066 nm with a slope efficiency η of 80% (with respect to P_{abs}). The laser threshold was at $P_{\text{abs}} = 1.5$ W and the optical-to-optical efficiency (with respect to P_{inc}) η_{opt} was 22%. For $T_{\text{OC}} = 5\%$, the laser performance only slightly deteriorated ($\eta = 79\%$) and for $T_{\text{OC}} = 10\%$, the increase of the laser threshold and the drop of η were noticeable. This is attributed to upconversion losses arising from both Tm^{3+} impurities present in the Yb_2O_3 reagent and Yb^{3+} - Yb^{3+} ion pairs. Indeed, the intensity of the blue (~ 480 nm) upconversion in the Yb^{3+} - Tm^{3+} system increased with T_{OC} . The laser output was linearly polarized (σ).

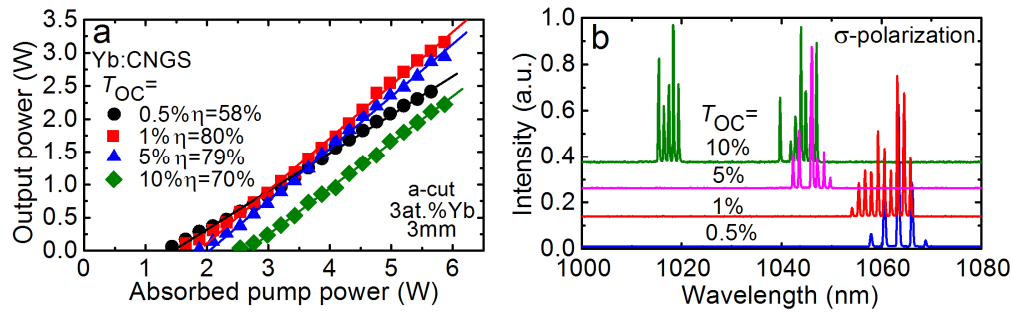


Fig. 5. Continuous-wave Yb:CNGS laser: (a) input-output dependences, η – slope efficiency; (b) typical laser emission spectra measured at $P_{\text{abs}} = 5.5$ W (a-cut crystal, 3 at.% Yb³⁺, 3 mm-thick).

The typical laser emission spectra are shown in Fig. 5(b). With the increase of T_{OC} (outcoupling losses), a blue-shift of the emission wavelength is observed in accordance with the σ_{g} spectra, Fig. 3(b). Remarkably, for $T_{\text{OC}} = 10\%$, laser oscillation in two spectral ranges, 1015-1019 nm and 1040-1047 nm, was observed, corresponding to two local maxima in the gain spectra. The multi-peak spectral behavior is due to the etalon effects arising from the small air gaps between crystal and resonator mirrors and is typical for microchip-type lasers.

Several Yb:CNGS samples with different Yb³⁺ doping and thickness t were studied using $T_{\text{OC}} = 1\%$, see Fig. 6. A summary of the output characteristics of these crystals and the corresponding values of A_{bs} are listed in Table 1. The laser output in all cases was σ -polarized.

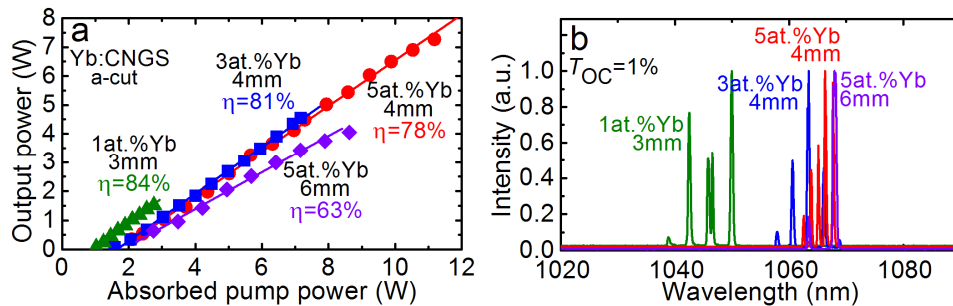


Fig. 6. Comparison of the laser performance of a-cut Yb:CNGS crystals with various Yb³⁺ doping levels ($T_{\text{OC}} = 1\%$, σ -polarization): (a) input-output dependences, η – slope efficiency; (b) typical laser emission spectra measured at maximum P_{abs} .

The maximum output power was achieved with a 4 mm-thick 5 at.% Yb:CNGS crystal, namely 7.27 W at 1062-1068 nm with $\eta = 78\%$. The laser threshold was at $P_{\text{abs}} = 1.7$ W and $\eta_{\text{opt}} = 39\%$. Even higher slope efficiency ($\eta = 84\%$) at lower threshold ($P_{\text{abs}} = 1.0$ W) was reached with a 3 mm-thick 1 at.% Yb:CNGS sample but the output lower (1.52 W) was limited by low absorption. In general, the increase of Yb³⁺ doping leads to the decrease of η due to increased internal losses in Yb:CNGS. These losses are caused by stronger lattice distortion with the Yb³⁺ incorporation. The internal losses in Yb:CNGS were estimated from the output performance of a 4 mm-thick 5 at.% Yb³⁺-doped crystal delivering the maximum output power, see Fig. 6(a), using a model of a quasi-three-level lasers [17], resulting in $\delta = 0.004 \pm 0.002$ cm⁻¹.

Table 1. Output Parameters of CW Yb:CNGS Lasers (*a*-cut, $T_{oc} = 1\%$).

Yb ³⁺ doping	<i>t</i> , mm	<i>Abs</i> , %	<i>P</i> _{out} , W	λ_{l_s} , nm	η , %	η_{opt} , %
1 at. %	3	20	1.52	1042-1050	84	11
3 at. %	3	41	3.16	1054-1066	80	22
	4	46	4.55	1058-1066	81	29
5 at. %	4	60	7.27	1062-1068	78	39
	6	68	4.05	1063-1068	63	32

The Yb:CNGS lasers generated a nearly circular output laser beam ($M_{x,y}^2 < 1.15$) for the whole range of studied P_{abs} , see Fig. 7. This is promoted by the weak anisotropy of thermal expansion, $\alpha_a/\alpha_c = 1.04$ [6]. The input-output dependences (Fig. 5 and Fig. 6) are clearly linear indicating no detrimental thermal effects. No damage of the crystal is observed in our experiments up to, at least, $P_{abs} = 11.2$ W. This is a remarkable result when considering the modest κ of this crystal which is lower even compared to the monoclinic Yb:KLuW and Yb:YCOB [16,18]. This is an indication of high stress fracture limit of CNGS.

Laser operation with an *a*-cut Yb:CNGS crystal in the microchip laser cavity indicates a positive thermal lens for this crystal cut. A direct measurement of the thermo-optic coefficient, dn/dT , of Yb:CNGS for σ -polarization also indicated a positive value, namely $dn_o/dT = 4.0 \times 10^{-6} \text{ K}^{-1}$ at $\sim 1 \mu\text{m}$ (unpublished).

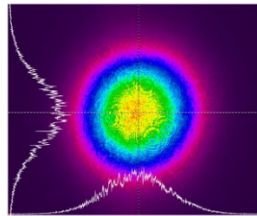


Fig. 7. 2D spatial intensity profile of the laser output from a CW Yb:CNGS laser (*a*-cut crystal, 5 at.% Yb³⁺, 4 mm-thick) measured at $P_{abs} = 11.2$ W.

4. Conclusion

In conclusion, we report on highly-efficient (slope efficiency $\sim 80\%$) multi-watt diode-pumped CW lasers based on a novel trigonal ordered silicate crystal, Yb:CNGS. Using a 5 at.% Yb:CNGS, a maximum output power of 7.27 W is extracted at 1062-1068 nm with $\eta = 78\%$. These are record parameters for $\sim 1 \mu\text{m}$ lasers based on this class of materials. CNGS offers relatively high Yb³⁺ doping levels, high transition cross-sections, and broad spectral bands. Moreover, a combination of the appropriate thermal and elastic characteristics makes Yb:CNGS a promising material for power-scalable lasers, in particular in microchip-like cavities due to its positive thermal lens [16]. Taking into account the long upper-laser-level lifetime of Yb³⁺ ions (0.71 ms), this crystal is suitable for PQS lasers employing Cr:YAG or V:YAG as saturable absorbers. By using a special crystal cut for type I or II phase-matching, self-frequency doubled lasers seems to be feasible [6]. Tunable and ultrashort pulse lasers at $\sim 1 \mu\text{m}$ can benefit from the broad and smooth gain cross section of Yb:CNGS.

Funding

Spanish Government (MAT2016-75716-C2-1-R, (AEI/FEDER,UE), MAT2013-47395-C4-4-R, TEC 2014-55948-R); Generalitat de Catalunya (2014SGR1358); National Natural Science Foundation of China (51472147, 61178060, 51672161).

Acknowledgments

F.D. acknowledges additional support through the ICREA academia award 2010ICREA-02 for excellence in research. X.M. acknowledges support from the European Union's Horizon 2020 research and innovation programme under the Marie Skłodowska-Curie grant agreement No 657630. P.L. acknowledges financial support from the Government of the Russian Federation (Grant 074-U01) through ITMO Post-Doctoral Fellowship scheme.